HHS Public Access

Author manuscript

Biomed Eng Adv. Author manuscript; available in PMC 2023 July 07.

Published in final edited form as:

Biomed Eng Adv. 2023 June ; 5: . doi:10.1016/j.bea.2023.100090.

Laser microgrooving and resorbable blast texturing for enhanced surface function of titanium alloy for dental implant applications

Sophie E. Jones,

Luke Nichols,

Steven H. Elder,

Lauren B. Priddy*

Department of Agricultural and Biological Engineering, Mississippi State University, Mississippi State, MS 39762, USA

Abstract

Long-term dental implant success is dependent on biocompatibility and osseointegration between the bone and the implant. Surface modifications such as laser-induced microgrooving which increase contact area can enhance osseointegration by establishing and directing a stable attachment between the implant surface and peri-implant bone. The objective of this study was to evaluate pre-osteoblast proliferation, morphology, and differentiation on titanium alloy (Ti64) surfaces—Laser-Lok© (LL), resorbable blast textured (RBT), and machined (M)—compared to tissue culture plastic (TCP) control. We hypothesized the LL surfaces would facilitate increased cellular alignment compared to all other groups, and LL and RBT surfaces would demonstrate enhanced proliferation and differentiation compared to M and TCP surfaces. Surface roughness was quantified using a surface profilometer, and water contact angle was measured to evaluate the hydrophilicity of the surfaces. Cellular function was assessed using quantitative viability and differentiation assays and image analyses, along with qualitative fluorescent (viability and cytoskeletal) imaging and scanning electron microscopy. No differences in surface roughness were observed between groups. Water contact angle indicated LL was the least hydrophilic surface, with RBT and M surfaces exhibiting greater hydrophilicity. Cell proliferation on day 2 was enhanced on both LL and RBT surfaces compared to M, and all three groups had higher cell numbers on day 2 compared to day 1. Cell orientation was driven by the geometry of the surface modification, as cells were more highly aligned on LL surfaces compared to TCP (on day 2) and RBT (on day 3). At day 21, cell proliferation was greater on LL, RBT, and TCP surfaces compared to M, though no differences in osteogenic differentiation were observed. Collectively, our results highlight the efficacy of laser microgrooved and resorbable blast textured surface modifications of Ti64 for enhancing cellular functions, which may facilitate improved osseointegration of dental implants.

*Corresponding author: Department of Agricultural and Biological Engineering, Mississippi State University, 130 Creelman Street, Mississippi State, MS 39762, USA. lbpriddy@abe.msstate.edu (L.B. Priddy).

Declaration of Competing Interest

The authors declare that they have no known competing financial interests or personal relationships that could have appeared to influence the work reported in this paper.

Keywords

Dental implants; Osseointegration; Surface properties; Bone-implant interface; Titanium

1. Introduction

Dental implants act as a replacement for the root of a missing tooth. Titanium is one of the most commonly used materials for dental implants due to its high mechanical strength and osseointegrative ability [1,2]. The most commonly used titanium alloy for dental implants is Ti-6Al-4V-ELI (Ti64), which consists of ~90% titanium, ~6% aluminum, ~4% vanadium, and extra low interstitials (ELI) [3]. Compared to dentures or dental bridges, implants better preserve the integrity of the teeth and gums and are more cost-effective and more permanent solutions for void bone volume than dentures or dental bridges [4,5]. It is estimated that two million dental implants are placed per year worldwide, yet 5% to 11% of these do not effectively integrate with the surrounding maxillofacial bone [6]. Long-term success of a dental implant is dependent on implant biocompatibility and osseointegration into the jawbone, which is defined as a direct structural and functional connection between ordered, living bone and the surface of a load-carrying implant [7]. This process is necessary for the implant to serve as a strong foundation for an artificial tooth, which should look and function like the original tooth [8].

Cell adhesion, proliferation, and osteogenic differentiation are critical cellular activities which initiate the process of osseointegration and may be predictive of osseointegration success [9]. Implant surface properties play a critical role in long-term outcomes, and surface modifications can be used to improve osseointegration by establishing a strong and stable attachment between the implant surface and the peri-implant bone [10]. The original dental implants are classified as machined, due to their smooth machined surface manufactured by turning, milling, or polishing [11,12]. As osteoblasts attach more readily to rougher Ti surfaces [2,13–17], dental implants with textured surfaces serve as an attractive alternative to traditionally machined implants which may limit cell attachment [9]. One method for introducing surface texture consists of exposing the Ti surface to rapid blasting, under pressure, with resorbable blast media (RBM). The resultant roughness has no preferred orientation and can be used to improve osseointegration by increasing surface area [18,19]. Roughened titanium surfaces produced by blasting or etching successfully improved proliferation and migration of osteoblast-like MG-63 cells compared to machined surfaces [17].

Laser-Lok, whereby cell-sized, parallel microchannels are laser-machined onto the surface of dental implants and abutments, facilitated contact guidance and cell alignment and promoted extracellular matrix growth in vitro [10,21]. These surface manufacturing techniques are applied to the implant collar, or neck of the dental implant [22]. More recently, these techniques have also been applied to the abutment, the portion of the dental implant in greater contact with the soft tissue [10]. A recent study comparing laser-grooved, alumina-blasted, and polished surfaces reported random cell orientations on blasted and smooth surfaces [20]. In contrast, laser grooved surfaces demonstrated contact guidance,

whereby the cells were oriented in the direction of the grooves, which can be advantageous for cell integration and adhesion purposes [20]. A study using Laser-Lok© (LL) showed elongated cells across the Laser-Lok surface, indicative of improved cell adhesion [10]. In a canine model, laser microgrooved surfaces implanted into the lateral metaphysis of the distal femur led to increased bone ingrowth compared to that in the alumina grit-blasted titanium alloy and alumina grit-blasted commercially pure titanium [23].

Maintaining crestal bone is another essential component to implant success [24]. Significant loss of crestal bone over time affects the load-bearing capacity of the implant and may lead to cosmetic problems and/or implant failure, especially for patients with poor bone quality [25]. A canine model demonstrated that laser microgrooved surfaces implanted into the bilateral mandibular premolar and first molar extraction sites had significantly more soft tissue attachment than machined or resorbable blast textured (RBT) surfaces [26]. This enhanced soft tissue attachment was associated with decreased apical migration of epithelial cells to the bone-tissue interface and maintenance of crestal bone [26–29]. Finite element analysis of stress in the critical crestal area of a dental implant suggested the increased surface area and more organized micro-textures of a Laser-Lok© collar may encourage bone integration and reduce crestal bone loss [30]. While previous studies have reported positive effects of laser microgrooved Ti64 surfaces on cellular behaviors [20,26,31], quantitative in vitro analyses are limited to date.

In this study, we evaluated the proliferation, morphology, and differentiation of pre-osteoblasts on laser-microgrooved Laser-Lok©, resorbable blast textured (RBT), and machined (M) Ti64 surfaces, compared to tissue culture plastic (TCP) controls. Outcome measures included cell proliferation, viability, morphology and orientation, and osteogenic differentiation. We hypothesized that LL and RBT surfaces would demonstrate enhanced proliferation and differentiation compared to M and TCP surfaces, and LL surfaces would facilitate increased alignment compared to all other groups.

2. Methods

2.1. Materials

Ti-6AL-4 V titanium alloy disks (10-mm diameter) were subjected to laser-microgrooved Laser-Lok© (LL), resorbable blast textured (RBT), or smooth, machined (M) surface modifications and were provided by BioHorizons Implant Systems, Inc. The LL microchannels were created using a proprietary laser ablation technology which produces repeatable, cell-sized, circumferential, parallel microchannels, along with a nanostructure to maximize surface area [10,21]. The RBT disks are blasted by RBM containing apatitic calcium phosphate particles and then cleaned to remove the particles [32]. For both the Laser-Lok© and RBT groups, samples from two production lots were included. The control for this study was Thermanox® tissue culture plastic (TCP) coverslips (13-mm diameter, Electron Microscopy Sciences).

2.2. Surface profilometry

Surface profilometry was used to visualize the surfaces of representative LL, RBT, M, and TCP disks. LL, RBT, and M disks were imaged via laser confocal imaging at 150X (Keyence VK-X1000). Due to its smooth surface, TCP was imaged with white light interferometry at 10X (Keyence VK-X3000). Surface profilometry was also used to quantify surface roughness (Sa), the arithmetical mean height over the scanned surface, and line roughness (Ra), of disk types LL, RBT, and M ($n = 5$) (Keyence VR-5000). For LL, RBT, and M disks, surface roughness was evaluated over a 2 × 2 mm section, and line roughness was measured along a 2-mm line, both on the upper middle half of the disk, to enable measurement of the microscale, engineered surface features rather than the global (~mm scale) patterns of the entire surface.

2.3. Water contact angle

Water contact angle measurements were completed for LL, RBT, and M ($n = 5$) surfaces using a CCD video camera (CUE, Camera Power Supply) along with ArcSoft ShowBiz to capture the images ImageJ (Fiji, NIH) was used to determine the contact angle.

2.4. Short-term cell proliferation and viability

MC3T3-E1 mouse pre-osteoblast cells (Subclone 4, ATCC®) were seeded at a density of 5000 cells per disk on all disk types (LL, RBT, M, and TCP). After incubation for 1 hour, 670 μL of growth medium was added to each well. Growth medium consisted of alpha minimum essential medium (Gibco) containing 10% fetal bovine serum (Atlanta Biologicals) and 1% penicillin-streptomycin (Gibco). A Cell Counting Kit-8 (CCK-8, Sigma-Aldrich) assay was run to observe cell attachment on day 1 and proliferation on days 2 and 3 ($n = 7–11$ per day), according to the manufacturer's protocol. Briefly, cells were incubated for 4 h with 90% growth media and 10% CCK-8 solution. The absorbance was read at 450 and 650 nm and converted to live cell counts using a standard curve. Live/dead staining with fluorescence microscopy was completed on days 1, 2, and 3 ($n = 2$ per day) to determine cell viability qualitatively. Samples were incubated in a phosphate buffered saline (PBS) containing 2 μM calcein AM and 4 μM ethidium homodimer-III solution at 37 °C for 15 min. Imaging was performed with a fluorescence microscope, where live cells appeared green and dead cells appeared red.

2.5. DAPI/phalloidin staining and analysis

Cell morphology and cytoskeletal (actin) orientation were assessed by DAPI/phalloidin staining with confocal laser scanning microscopy on days 1, 2, and 3. Samples ($n = 2–3$ per day) were fixed in 3.5% formaldehyde overnight prior to staining. Phalloidin and DAPI staining solutions were prepared before use in the staining steps. A 400X stock solution (equivalent to ~66 μM) was prepared by dissolving a vial of Alexa Fluor 488 Phalloidin (300 units, Invitrogen) in 150 μL dimethyl sulfoxide (DMSO, Sigma-Aldrich). DAPI staining solution was prepared by aliquoting stock DAPI (Invitrogen D3571) to 5 mg/mL and freezing at ~20 °C; when time for staining, the necessary number of aliquots were diluted with 1.5 mL PBS to a desired concentration of 40 μg/mL. The fixative was removed from the samples, and after lysing cells with 0.5% Triton X-100, blocking non-specific binding

with 1% bovine serum albumin (Sigma), and rinsing samples with PBS between steps, 700 μL of 165 nM (400X stock diluted 1:400 in PBS) phalloidin stain solution (Fisher Scientific) was placed in the wells and incubated at room temperature for 20 min (protected from light) to stain the actin cytoskeleton. Phalloidin stain was then removed, samples were rinsed with PBS, and DAPI staining solution (Fisher Scientific) was added to the wells and incubated for 30 min at room temperature (protected from light) to stain the nuclei. Samples were then observed under a confocal laser scanning microscope (Zeiss LSM 510).

Cytoskeletal angle of alignment was analyzed and quantified using the directionality analysis tool in Fiji (NIH). Three images from each of two disks ($n = 6$ total) were analyzed to yield values of angular direction and angular dispersion. The direction angle (°) indicated the mean angle of cytoskeletal alignment on each disk surface, and the dispersion angle (°) represented the variance in alignment across each surface. To account for any differences in orientation of the surface textures of disks during imaging, for each disk, the median direction angle of the three images was adjusted to 0° by subtraction, and the other two angles were adjusted by subtracting that same median angle, according to the following equation:

Original angle (°) – Median angle of 3 images (°) = Adjusted angle (°)

2.6. Scanning electron microscopy (SEM)

SEM imaging was performed on the samples used for live/dead imaging on days 1, 2, and 3 ($n = 2$ per day) to further characterize cell morphology and alignment. Following live/dead staining and imaging, samples were rinsed with PBS and fixed in 2.5% glutaraldehyde. Samples were then soaked in increasingly concentrated ethanol solutions (20–100%), then in hexamethyldisilazane (HMDS, Electron Microscopy Sciences) to completely dry the samples. Finally, samples were sputter coated with 90-nm gold nanoparticles before being imaged with a Zeiss EVO-50 Variable Pressure SEM.

2.7. Long-term proliferation and osteogenic differentiation

On day 0, LL, RBT, M, and TCP disks were seeded with 2500 mouse pre-osteoblast cells (MC3T3-E1) in 30 μL growth medium in 24-well plates for 2 h and then supplemented with additional growth medium for another 2 h. Following the initial 4 h of incubation, the growth media was replaced with differentiation media, except for TCP wells which were exposed to growth medium throughout the entire experiment (TCP growth). Growth medium consisted of alpha minimum essential medium (Gibco) containing 10% fetal bovine serum (Atlanta Biologicals) and 1% penicillin-streptomycin. Differentiation media comprised growth medium with the addition of 10 nM dexamethasone (Sigma) and 10 mM β-glycerophosphate (EMD Millipore Corp) [33,34]. Media was changed every other day.

On days 7, 14, and 21, cell proliferation and differentiation were measured ($n \geq 6$ per group per time point), with separate samples used for each time point (i.e., no repeated measures). First, cell proliferation was measured using a CCK-8 assay (Sigma, 96,992) as described previously. To measure differentiation, disks were moved to a 48-well plate to ensure complete coverage of each disk with the solution. 100 μL of lysis buffer (0.5% Triton X-100 prepared in PBS) was added to each well and the cells were incubated for 20 min.

200 μL of alkaline phosphatase substrate solution (0.072 gs of para-Nitrophenylphosphate powder in 25 mL of tris buffer (0.197 gs of Trizma powder and 25 mL of water adjusted to a pH of 10.3)) was added to each well, and the cells were incubated for 1 hour. Lastly, 100 μL of stop solution (0.2 M NaOH) was added to stop the reaction. The absorbance was read at 405 nm and converted to ALP activity using a standard curve [35].

2.8. Statistical analyses

Surface roughness and water contact angle were analyzed using a one-way analysis of variance (ANOVA) with Tukey's post-hoc pairwise comparisons using GraphPad Prism 8 (GraphPad Software, Inc.). Cell proliferation, cytoskeletal directionality, cytoskeletal dispersion, and cell differentiation data were analyzed by SAS (SAS 9.4) using a mixed model and repeated measures. An unstructured covariance matrix model was used when the model converged, and an autoregressive model was used when model did not converge. Pairwise comparisons were analyzed via Tukey's corrections. An alpha value of 0.05 was used for all statistical analyses.

Initially for all cellular analyses, the two LL and RBT lots were analyzed as separate groups with the rest of the samples in a two-way ANOVA. There was no effect of lot for either surface treatment, so for all analyses reported here, samples from both LL lots were grouped together, and samples from both RBT lots were grouped together, resulting in double the sample size for these two groups. All data are presented as mean ± standard deviation.

3. Results

3.1. Surface profilometry

Surface profilometry demonstrated the variations in surface topographies of LL, RBT, M, and TCP (Fig. 1). The grooves in LL, ~7–8 μm deep, are easily visualized, as is the roughness of RBT. The minimal texture of M compared to LL and RBT is distinguishable. Of note, LL, RBT, and M topographies are all presented on the same micrometer scale, whereas the TCP surface profile is shown on a nanometer scale, demonstrating its expectedly flat and smooth surface. Quantitatively, no differences in surface roughness (Sa, arithmetical mean height) or line roughness (Ra) were observed (Fig. 2).

3.2. Water contact angle

Water contact angle measurements showed that LL had the highest contact angle (115.1°), followed by RBT (85.08°); M was the most hydrophilic surface modification with a contact angle of 68.98° (Fig. 3). All pairwise comparisons were significantly different.

3.3. Short-term cell proliferation and viability

On day 2, cell numbers on both LL and RBT were greater than M, and RBT was greater than TCP (Fig. 4). Cell number on LL, RBT, and M increased significantly from day 1 to day 2. The live/dead staining of day 1 gave a visual representation of cell attachment on the various surface modifications (Fig. 5). The LL surface elicited a more organized attachment of cells. RBT demonstrated prevalent attachment but showed less organization than LL. Cells on M disks appeared to attach more readily to the center of the disk, and cells on TCP

disks were visibly reduced in number compared to the other groups. For all groups, cells that attached to the surfaces appeared viable, with little to no dead cells observed.

3.4. DAPI/phalloidin staining and analysis

As expected, cell orientation was driven by the geometry of the surface modification. Similarly, to the live/dead staining, DAPI/phalloidin images demonstrated the cells' tendency to organize along the grooves of a surface (Fig .6). This preferred orientation was observed primarily in the LL images as early as day 1. The cells also adhered to and spread on the surfaces of RBT and TCP, but in a more randomized fashion. Surprisingly, cells on M disks exhibited a preferred orientation by day 2. Though cytoskeletal direction on average was similar for all groups, cytoskeletal direction on LL was consistently close to zero with low variability at all time points (Fig. 7). On day 2, LL had lower cytoskeletal dispersion compared to TCP, and on day 3, LL had lower cytoskeletal dispersion compared to RBT.

3.5. Scanning electron microscopy (SEM)

Cells flourished especially on the rougher LL and RBT surfaces, indicated by spreading/filopodia (Fig. 8). Cells adhered along and within the LL channels. Similarly, cells adhered to RBT in a 3D/textured fashion, but no preferred orientation was observed.

3.6. Long-term proliferation and osteogenic differentiation

At day 7, no differences in cell proliferation were observed (Fig. 9). As expected, cell numbers increased for each group from day 7 to day 14, but the only significant increase was in the RBT group. RBT also displayed higher proliferation at day 21 than on day 14. At day 21, proliferation on M was lower than for all other groups.

ALP activity was negligible at day 7. At day 14 and 21, ALP activity was observed but no differences were measured between groups.

4. Discussion

As physicochemical properties of a biomaterial surface such as topography and wettability influence adhesion, proliferation, and differentiation of cells on the surface [9,10,17,36], surface modifications that enhance these cellular processes would be expected to improve long-term stability and success of an implant [37]. Collectively, our results indicate the topographies of Laser-Lok© (LL) and resorbable blast textured (RBT) surfaces promoted better attachment, proliferation, and differentiation of pre-osteoblasts compared to machined (M) and tissue culture plastic (TCP) surfaces. Enhancement of these cell functions on rough implant surfaces compared to smooth surfaces is known to facilitate better osseointegration [13]. Compared to M and TCP surfaces, improved short-term proliferation on LL and RBT surfaces was observed, likely due to the increased surface area and promotion of a three-dimensional cellular network on LL and RBT [19,38]. The LL topography consists of lasered microchannels with an average line roughness (Ra) of 1.25 μm and groove depths of ~7–8 μm, which correspond to the Ra of 1.33 μm [10] and grooves 6–12 μm deep [30] reported previously. The higher proliferation of cells on LL was presumably not influenced

by surface roughness, as Sa was equivalent between LL, RBT, and M. No surfaces exhibited cytotoxic effects, as indicated by a lack of dead cells in live/dead staining. Surprisingly, the water contact angle results indicated LL was the least hydrophilic and M was the most hydrophilic of the three Ti64 surfaces. The relative hydrophobicity of LL may be due to the space/ridges between the grooves acting as a barrier to the water, a phenomenon which has also been observed of butterfly wings with ridges of similar micron-scale [39]. Nonetheless, the superior cell attachment and proliferation on LL is believed to be based on the guidance of cell spreading by the LL surface topography, which has been shown to direct cell migration and can lead to contact guidance on the implant surface [40].

To our knowledge, this is the first study quantitatively comparing osteogenic differentiation on laser microgrooved, resorbable blast textured, and machined Ti64 surfaces. Our results demonstrate enhanced cell differentiation on LL and RBT surfaces compared to TCP control (growth media) at day 21. Others have also found that laser microgrooved Ti surfaces facilitated superior osteogenic differentiation compared to untreated Ti surfaces, as indicated by increased ALP and calcium production, and RUNX2, OPN, BMP-2, and ALP gene expression [41]. Further, grooved (600 grit) and rough (sandblasted) surfaces resulted in increased RUNX2 and osteocalcin gene expression compared to those from cells on TCP [42]. Throughout the extended (21-day) proliferation study, LL and RBT promoted relatively high proliferation and differentiation, while both TCP groups (osteogenic and growth medium) exhibited high proliferation but little differentiation. Interestingly, the osteogenic medium alone was insufficient to promote high levels of differentiation on TCP at any time point, suggesting the surface features of LL and RBT may have elicited an enhancing effect on differentiation. Additionally, cells on M surfaces exhibited low proliferation at days 14 and 21, and minimal differentiation at day 21. The day 7 proliferation was similar among all groups, indicating the lack of proliferation on M surfaces later was not due to lack of attachment or early growth, but may instead be a result of the cells reaching confluency earlier due to a more limited surface area available.

DAPI/phalloidin images indicated more highly aligned cells on LL surfaces. Directionality data from these images further revealed more consistently aligned cells across the LL surfaces than any other group, indicated by both directionality close to zero and lower dispersion. Previously, laser microgrooved surfaces provided contact guidance and promoted extracellular matrix growth compared to alumina-blasted and polished surfaces [20], which may explain the reduction in scar tissue formation and fibrous encapsulation on LL surfaces observed in another study [40]. Results from a unique model in which textured coupons were loaded within implantable chambers placed in the canine distal femur suggested laser microgrooved surfaces more effectively controlled the direction of bone ingrowth and resulted in a stronger bone-implant interface compared to alumina grit-blasted surfaces [23]. Laser microgrooved implants have also been shown to reduce crestal bone resorption by preventing epithelial downgrowth and improving soft tissue healing [29]. SEM imaging further demonstrated morphology of the cells on each surface type. Given more points of contact on which to adhere, cells on the LL surface were aligned in the LL grooves and extended filipodia between ridges of the topography. In contrast, the RBT surfaces induced more randomly oriented cells due to lack of any oriented texture (e.g., grooves). However, except for higher cell number on LL (versus all groups, including RBT) at day 3, this lack of

orientation on RBT surfaces did not affect cell proliferation or differentiation, as these were equivalent between LL and RBT at all other time points. Future work involving elemental analyses would provide valuable information on the extent and distribution of mineralization by differentiating cells.

5. Conclusion

Physical modifications of an implant surface can establish and direct a stable attachment between the implant surface and the peri-implant bone and subsequently facilitate osseointegration. In this study, proliferation of pre-osteoblasts on LL and RBT surfaces was greater compared to traditional M and TCP surfaces. Cells on LL surfaces also exhibited increased alignment, driven by the geometry of the surface modification. While no differences in surface roughness were found, LL and RBT surfaces were surprisingly less hydrophilic than traditional M surfaces, suggesting the improved cellular proliferation is due to other qualities of the surface modification. Collectively, laser microgrooved and resorbable blast textured surface modifications on dental implants enhanced cellular proliferation and alignment, which may promote implant osseointegration and ultimately long-term success of dental implants.

Acknowledgments

Thank you to Rana Atieh for input on the study design and to Luke Tucker for assistance with statistical analyses.

Funding

This work was supported by BioHorizons Implant Systems, Inc., as well as the Office of Research and Economic Development and Bagley College of Engineering at Mississippi State University. L. Priddy is supported in part by the National Institutes of Health [P20GM103646].

Data availability

Data will be made available on request.

Abbreviations:

Ti64	Ti-6Al-4V-ELI
ELI	Extra low interstitials
RBM	resorbable blast media
LL	Laser-Lok
RBT	resorbable blast textured
M	machined
TCP	tissue culture plastic
CCK-8	Cell Counting Kit-8
HMDS	hexamethyldisilazane

References

[1]. Kaur M, Singh K, Review on titanium and titanium based alloys as biomaterials for orthopaedic applications, Mater. Sci. Eng. C 102 (2019) 844–862, 10.1016/J.MSEC.2019.04.064.

[2]. Dobrzański LA, Dobrzański LB, Achtelik-Franczak A, Dobrzańska J, Application solid laser-sintered or machined Ti6Al4V alloy in manufacturing of dental implants and dental prosthetic restorations according to dentistry 4.0 concept, Process (2020) 664 2020, 10.3390/PR8060664. Vol 8, Page 8:664.

[3]. Nicholson JW Titanium Alloys for Dental Implants: a Review 2023 n.d. 10.3390/prosthesis2020011.

[4]. Gupta R, Gupta N, Weber KK, Dental implants, Bioceram Calcium Phosphate (2021) 115–130, 10.1201/9781351070133.

[5]. Popelut A, Valet F, Fromentin O, Thomas A, Bouchard P, Relationship between Sponsorship and Failure Rate of Dental Implants: a Systematic Approach, PLoS One 5 (2010) e10274, 10.1371/JOURNAL.PONE.0010274. [PubMed: 20422000]

[6]. Han DK, Accioni F, Vázquez J, Merinero M, Begines B, Alcudia A, Latest trends in surface modification for dental implantology, Innov. Develop. Anal. Appl (2022), 10.3390/pharmaceutics14020455.

[7]. Anil S, Anand PS, Alghamdi H, Jansen JA 4 Dental implant surface enhancement and osseointegration 2023 n.d.

[8]. Bressan E, Sbricoli L, Guazzo R, Tocco I, Roman M, Vindigni V, et al. , Nanostructured surfaces of dental implants, Int. J. Mol. Sci 14 (2013) 1918–1931, 10.3390/IJMS14011918. [PubMed: 23344062]

[9]. Chen S, Guo Y, Liu R, Wu S, Fang J, Huang B, et al. , Tuning surface properties of bone biomaterials to manipulate osteoblastic cell adhesion and the signaling pathways for the enhancement of early osseointegration, Colloids Surfaces B Biointerf. 164 (2018) 58–69, 10.1016/J.COLSURFB.2018.01.022.

[10]. Esfahanizadeh N, Motalebi S, Daneshparvar N, Akhoundi N, Bonakdar S, Morphology, proliferation, and gene expression of gingival fibroblasts on Laser-Lok, titanium, and zirconia surfaces, Lasers Med. Sci 31 (2016) 863–873, 10.1007/SI0103-016-1927-6/FIGURES/9. [PubMed: 27025859]

[11]. Matos GRM, Surface roughness of dental implant and osseointegration, J. Maxillofac. Oral Surg 20 (2020) 1–4, 10.1007/S12663-020-01437-5, 2020 201. [PubMed: 33584035]

[12]. Abraham CM, Suppl 1: a brief historical perspective on dental implants, their surface coatings and treatments, Open Dent. J 8 (2014) 50, 10.2174/1874210601408010050. [PubMed: 24894638]

[13]. Barfeie A, Wilson J, Rees J Implant surface characteristics and their effect on osseointegration 2015. 10.1038/sj.bdj.2015.171.

[14]. Velasco-Ortega E, Alfonso-Rodríguez CA, Monsalve-Guil L, España-López A, Jiménez-Guerra A, Garzón I, et al. , Relevant aspects in the surface properties in titanium dental implants for the cellular viability, Mater. Sci. Eng. C 64 (2016) 1–10, 10.1016/J.MSEC.2016.03.049.

[15]. Teng FY, Ko CL, Kuo HN, Hu JJ, Lin JH, Lou CW, et al. , A comparison of epithelial cells, fibroblasts, and osteoblasts in dental implant titanium topographies, Bioinorg. Chem. Appl (2012), 10.1155/2012/687291,2012.

[16]. Boyan BD, Lossdórfer S, Wang L, Zhao G, Lohmann CH, Cochran DL, et al. , Osteoblasts generate an osteogenic microenvironment when grown on surfaces with rough microtopographies, Eur. Cell Mater 6 (2003) 22–27, 10.22203/ECM.V006A03. [PubMed: 14577052]

[17]. Nishimoto SK, Nishimoto M, Park S-W, Lee K-M, Kim H-S, Koh J-T, et al. , The effect of titanium surface roughening on protein absorption, cell attachment, and cell spreading, Int. J. Oral Maxillofac. Implants 23 (2008) 675–680. [PubMed: 18807564]

[18]. Witek L, Marin C, Granato R, Bonfante EA, Campos FEB, Gomes JB, et al. , Surface characterization, biomechanical, and histologic evaluation of alumina and bioactive resorbable

blasting textured surfaces in titanium implant healing chambers: an experimental study in dogs, Int. J. Oral Maxillofac. Implants 28 (2013) 694–700, 10.11607/JOMI.2952. [PubMed: 23748299]

[19]. Galli S, Jimbo R, Tovar N, Yoo DY, Anchieta RB, Yamaguchi S, et al. , The effect of osteotomy dimension on osseointegration to resorbable media-treated implants: a study in the sheep, J. Biomater. Appl 29 (2015) 1068–1074, 10.1177/0885328214553958. [PubMed: 25281647]

[20]. Soboyejo WO, Nemetski B, Allameh S, Marcantonio N, Mercer C, Ricci J, Interactions between MC3T3-E1 cells and textured Ti6Al4V surfaces, J. Biomed. Mater. Res 62 (2002) 56–72, 10.1002/JBM.10221. [PubMed: 12124787]

[21]. Jain V, Bhandari A, Vats N, Bhandari R, Goyal A, Srivastav V, Dental implant surface: driving force for successful osseointegration. Website WwwIjrrjournalCom, Orig. Res. Artic. Int. J. Res. Rev 7 (2020) 454, 10.4444/ijrr.1002/2345.

[22]. Smeets R, Stadlinger B, Schwarz F, Beck-Broichsitter B, Jung O, Precht C, et al. Impact of Dental Implant Surface Modifications on Osseointegration 2016. 10.1155/2016/6285620.

[23]. Frenkel SR, Simon J, Alexander H, Dennis M, Ricci JL, Osseointegration on metallic implant surfaces: effects of microgeometry and growth factor treatment, J. Biomed. Mater. Res 63 (2002) 706–713, 10.1002/JBM.10408. [PubMed: 12418014]

[24]. Gultekin BA, Sirali A, Gultekin P, Yalcin S, Mijiritsky E, Does the laser-microtextured short implant collar design reduce marginal bone loss in comparison with a machined collar? Biomed. Res. Int (2016) 10.1155/2016/9695389, 2016.

[25]. Misch CE, Perel ML, Wang HL, Sammartino G, Galindo-Moreno P, Trisi P, et al. , Implant success, survival, and failure: the International Congress of Oral Implantologists (ICOI) pisa consensus conference, Implant Dent. 17 (2008) 5–15, 10.1097/ID.0B013E3181676059. [PubMed: 18332753]

[26]. Nevins M, Kim DM, Jun S-H, Guze K, Schupbach P, Nevins ML, Histologic evidence of a connective tissue attachment to laser microgrooved abutments: a canine study, Int. J. Periodontics Restorative Dent 30 (2010) 245–255. [PubMed: 20386781]

[27]. Blézquez-Hinarejos M, Ayuso-Montero R, Jané-Salas E, López-López J, Influence of surface modified dental implant abutments on connective tissue attachment: a systematic review, Arch. Oral. Biol 80 (2017) 185–192, 10.1016/J.ARCHORALBIO.2017.04.020. [PubMed: 28456116]

[28]. Iglhaut G, Becker K, Golubovic V, Schliephake H, Mihatovic I, The impact of dis-/reconnection of laser microgrooved and machined implant abutments on soft- and hard-tissue healing, Clin. Oral. Implants Res 24 (2013) 391–397, 10.1111/CLR.12040. [PubMed: 23009248]

[29]. Chien HH, Schroering RL, Prasad HS, Tatakis DN, Effects of a new implant abutment design on peri-implant soft tissues, J. Oral Implantol 40 (2014) 581–588, 10.1563/AAID-JOI-D-12-00313. [PubMed: 23339331]

[30]. Alexander H, Ricci JL, Hrico GJ, Mechanical basis for bone retention around dental implants, J. Biomed. Mater. Res. Part B Appl. Biomater 88B (2009) 306–311, 10.1002/JBM.B.30845.

[31]. Zheng Q, Mao L, Shi Y, Fu W, Hu Y Biocompatibility of Ti-6Al-4V titanium alloy implants with laser microgrooved surfaces. 2020. 10.1080/10667857.2020.1816011.

[32]. Scarano A, Perrotti V, Artese L, Degidi M, Degidi D, Piattelli A, et al. , Blood vessels are concentrated within the implant surface concavities: a histologic study in rabbit tibia, Odontology 102 (2014) 259–266, 10.1007/S10266-013-0116-3. [PubMed: 23783569]

[33]. Qi H, Ye Z, Ren H, Chen N, Zeng Q, Wu X, et al. , Bioactivity assessment of PLLA/PCL/HAP electrospun nanofibrous scaffolds for bone tissue engineering, Life Sci. 148 (2016) 139–144, 10.1016/JXFS.2016.02.040. [PubMed: 26874032]

[34]. Li L, Yao L, Wang H, Shen X, Lou W, Huang C, et al. , Magnetron sputtering of strontium nanolayer on zirconia implant to enhance osteogenesis, Mater Sci Eng C 127 (2021), 112191, 10.1016/J.MSEC.2021.112191.

[35]. Priddy LB, Chaudhuri O, Stevens HY, Krishnan L, Uhrig BA, Willett NJ, et al. , Oxidized alginate hydrogels for bone morphogenetic protein-2 delivery in long bone defects, Acta Biomater 10 (2014) 4390–4399, 10.1016/J.ACTBIO.2014.06.015. [PubMed: 24954001]

[36]. Goriainov V, Cook R, Latham JM, Dunlop DG, Oreffo ROC, Bone and metal: an orthopaedic perspective on osseointegration of metals, Acta Biomater. 10 (2014) 4043–4057, 10.1016/J.ACTBIO.2014.06.004. [PubMed: 24932769]

[37]. Nobles KP, Janorkar AV, Williamson RS, Surface modifications to enhance osseointegration-resulting material properties and biological responses, J. Biomed. Mater. Res. Part B Appl. Biomater 109 (2021) 1909–1923, 10.1002/JBM.B.34835.

[38]. Kim HK, Jang JW, Lee CH, Surface modification of implant materials and its effect on attachment and proliferation of bone cells, J. Mater. Sci. Mater. Med 15 (2004) 825–830, 10.1023/B:JMSM.0000032824.62866.Al, 2004 157. [PubMed: 15387419]

[39]. Watson GS, Green DW, Schwarzkopf L, Li X, Cribb BW, Myhra S, et al. , A gecko skin micro/nano structure – a low adhesion, superhydrophobic, anti-wetting, self-cleaning, biocompatible, antibacterial surface, Acta Biomater. 21 (2015) 109–122, 10.1016/J.ACTBIO.2015.03.007. [PubMed: 25772496]

[40]. Bone response to laser microtextured surfaces | Semantic Scholar n.d 2023.

[41]. Wang C, Hu H, Li Z, Shen Y, Xu Y, Zhang G, et al. , Enhanced osseointegration of titanium alloy implants with laser microgrooved surfaces and graphene oxide coating, ACS Appl. Mater. Interfaces 11 (2019) 39470–39483, 10.1021/ACSAMI.9B12733/ASSET/IMAGES/LARGE/AM9B12733_0004.JPEG. [PubMed: 31594306]

[42]. Schneider GB, Zaharias R, Seabold D, Keller J, Stanford C, Differentiation of preosteoblasts is affected by implant surface microtopographies, J. Biomed. Mater. Res. Part A 69A (2004) 462–468, 10.1002/JBM.A.30016.

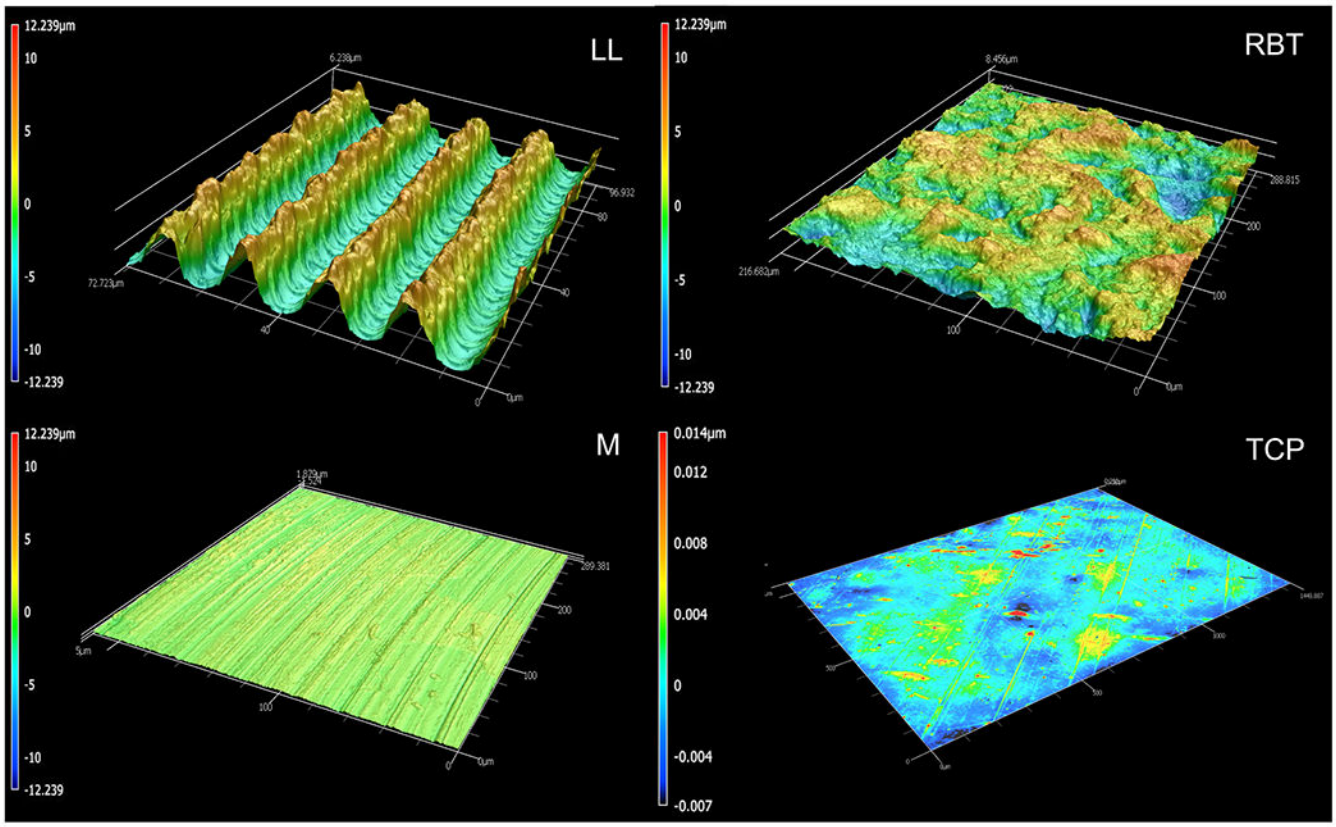

Fig. 1.

Surface profilometry scans of Laser-Lok (LL), resorbable blast textured (RBT), machined (M), and tissue culture plastic (TCP) surfaces. Note: different scale bar for TCP enables visualization of smaller scale features.

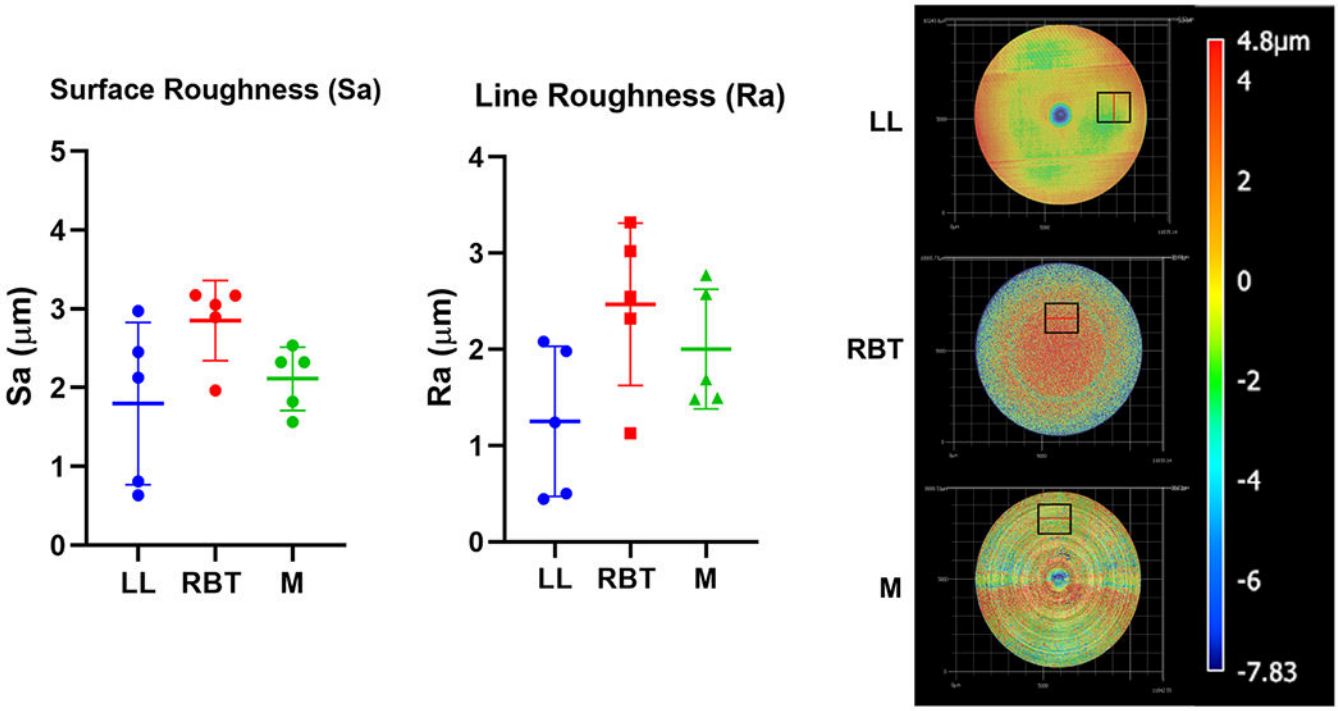

Fig. 2.

Surface profilometry quantification of surface (area) roughness (Sa, within black box) and line roughness (Ra, along red line inside black box) of Laser-Lok (LL), resorbable blast textured (RBT), and machined (M) surfaces ($n = 5$). There were no significant differences (α=0.05) between groups.

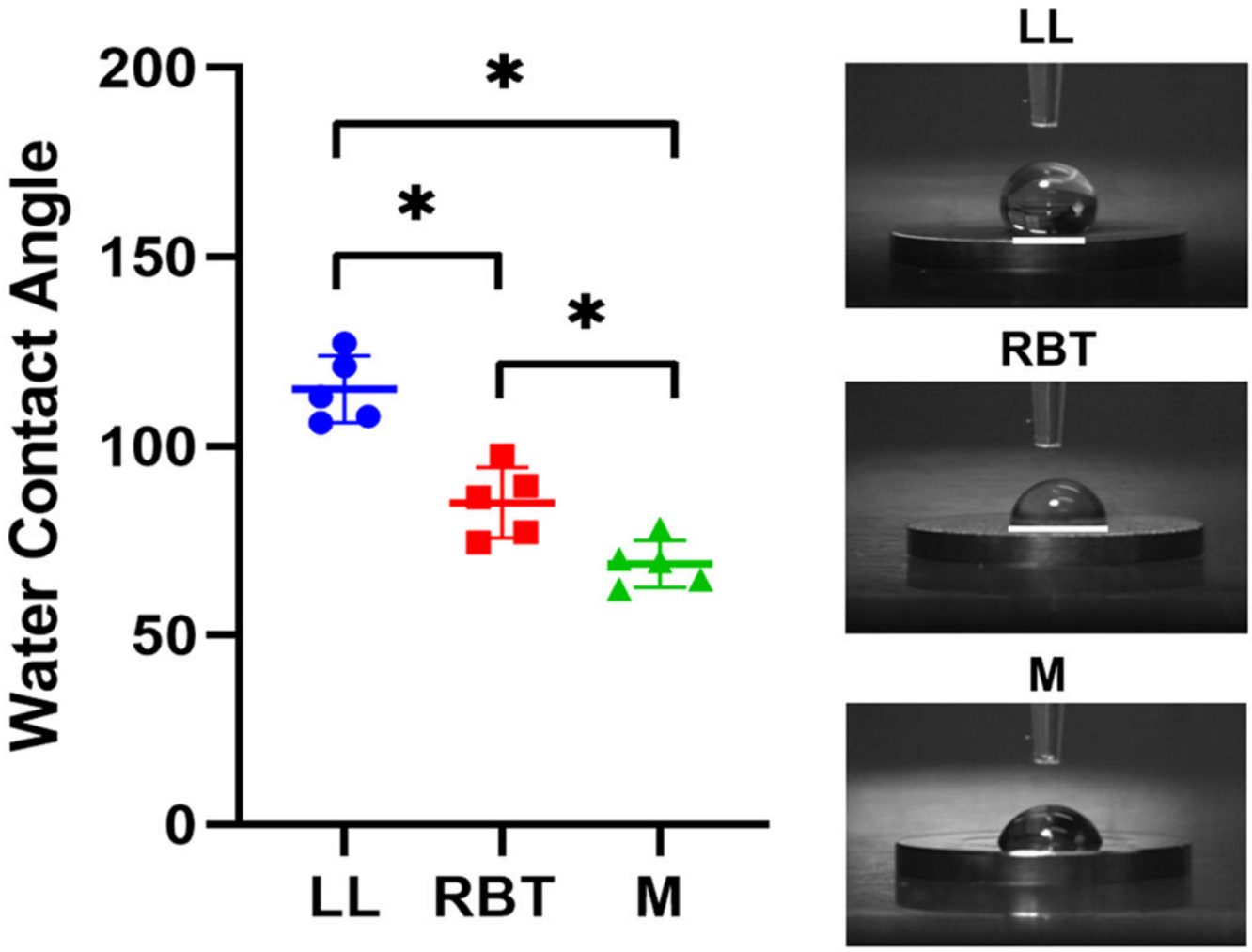

Fig. 3.

Water contact angle measurements for LL, RBT, and M ($n = 5$). Representative images from each group shown. (*) indicates significant difference ($p<0.05$).

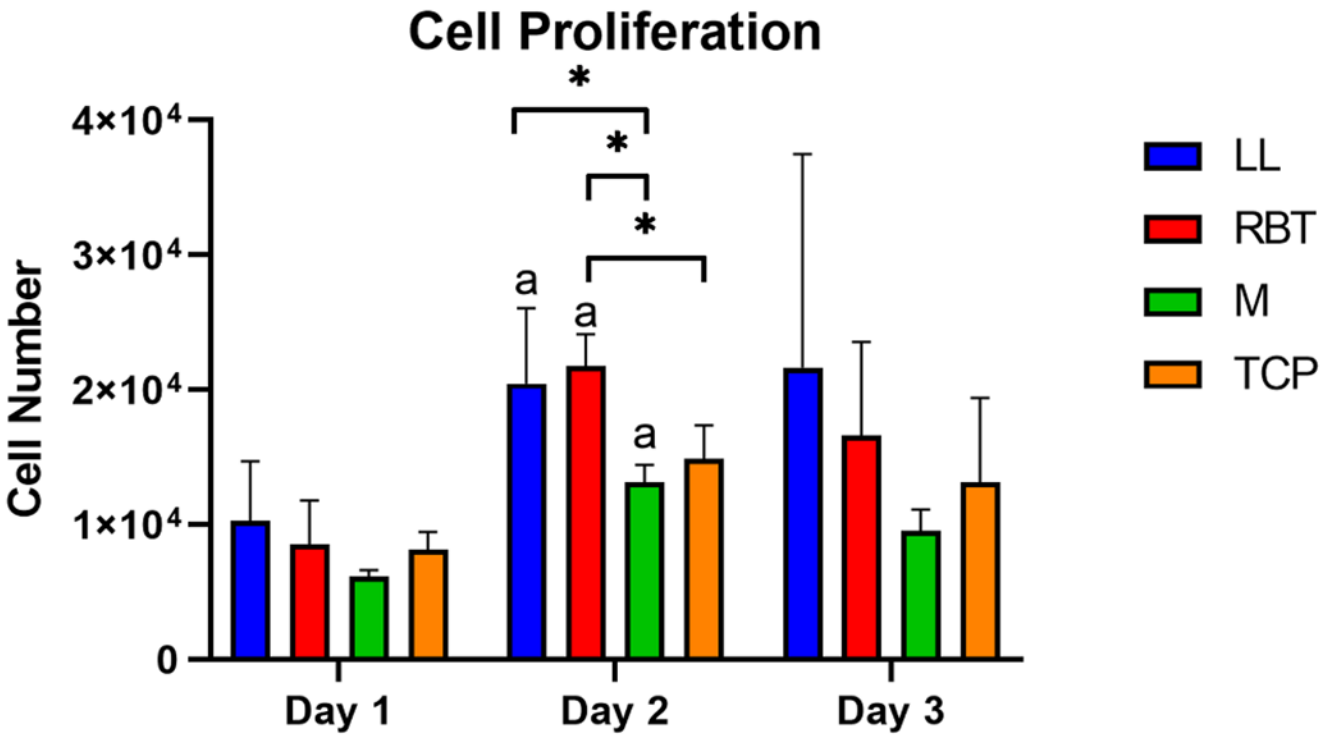

Fig. 4.

Cell number for pre-osteoblasts on LL ($n = 10$), RBT ($n = 10$), M ($n = 5$), and TCP ($n = 5$) at days 1, 2, and 3. (*) indicates significant difference between groups within a time point, (a) indicates significant difference to day 1 within that group ($p<0.05$). 5000 cells were seeded at day 0.

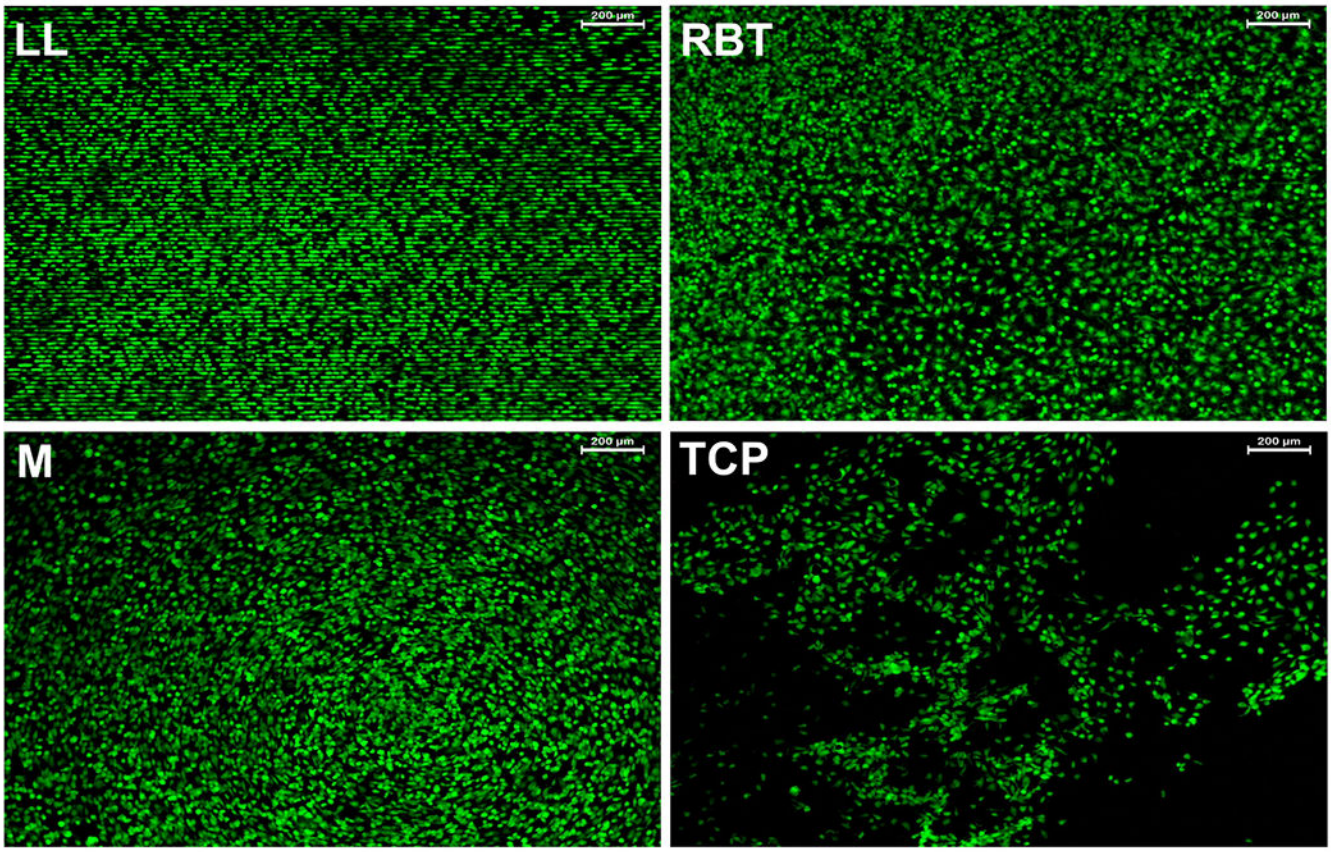

Fig. 5.
Live/dead staining of pre-osteoblasts on representative samples at day 1. (green = live cells, red = dead cells).

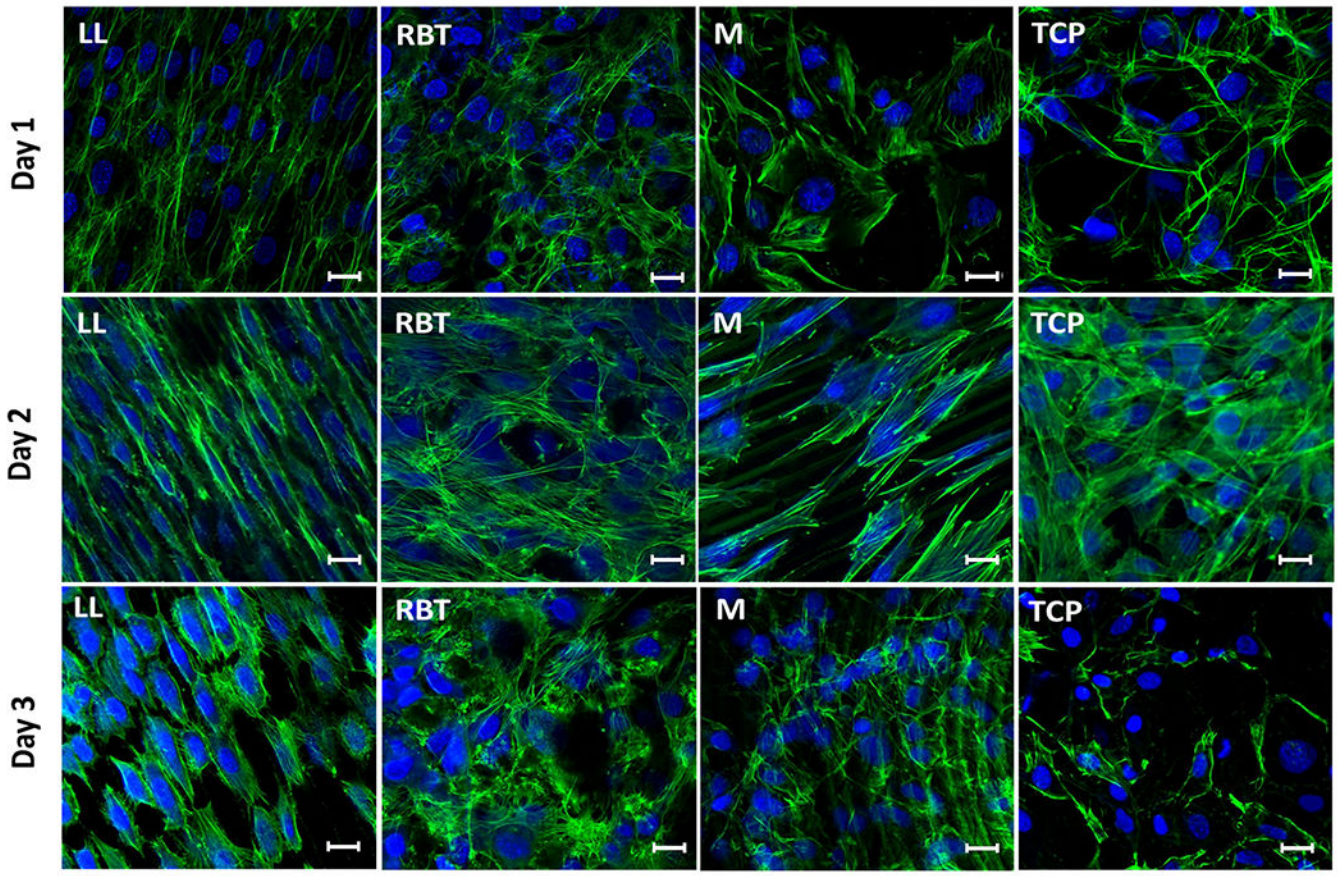

Fig. 6.

DAPI/phalloidin staining with confocal imaging of pre-osteoblasts on a representative sample from each group on days 1, 2, and 3. (blue = nuclei, green = actin cytoskeleton) (scale bar = 20 μm).

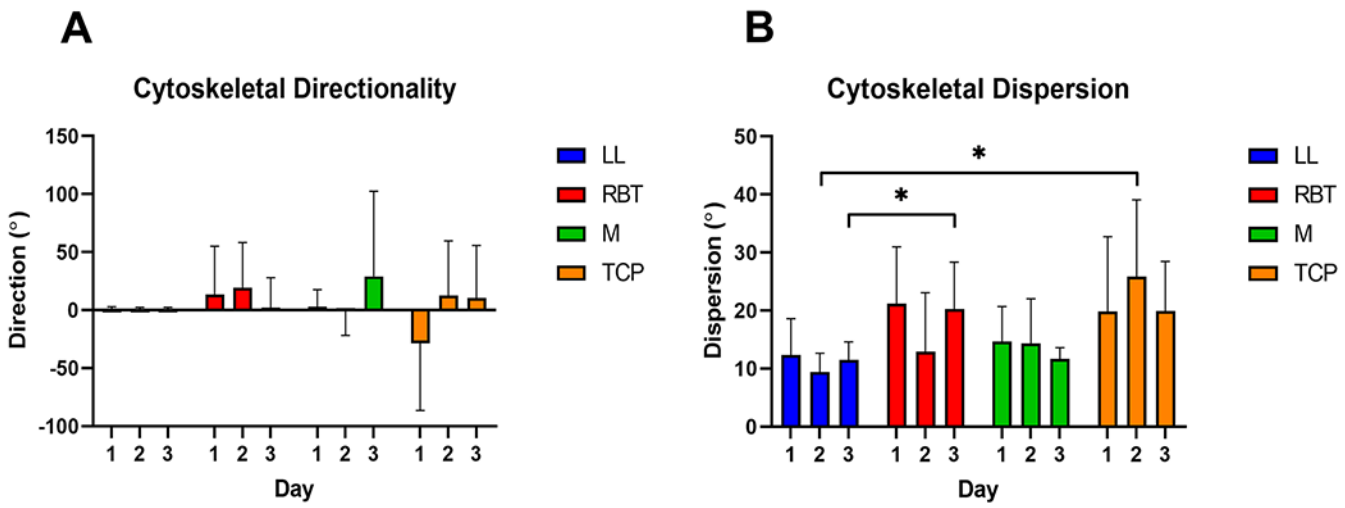

Fig. 7.

(A) Cytoskeletal directionality from DAPI/phalloidin images. There were no significant differences (α=0.05) between groups. (B) Cytoskeletal dispersion from DAPI/phalloidin images. (*) indicates significant difference between groups within a time point (p<0.05). (n = 6 for M and TCP, n = 12 for LL and RBT).

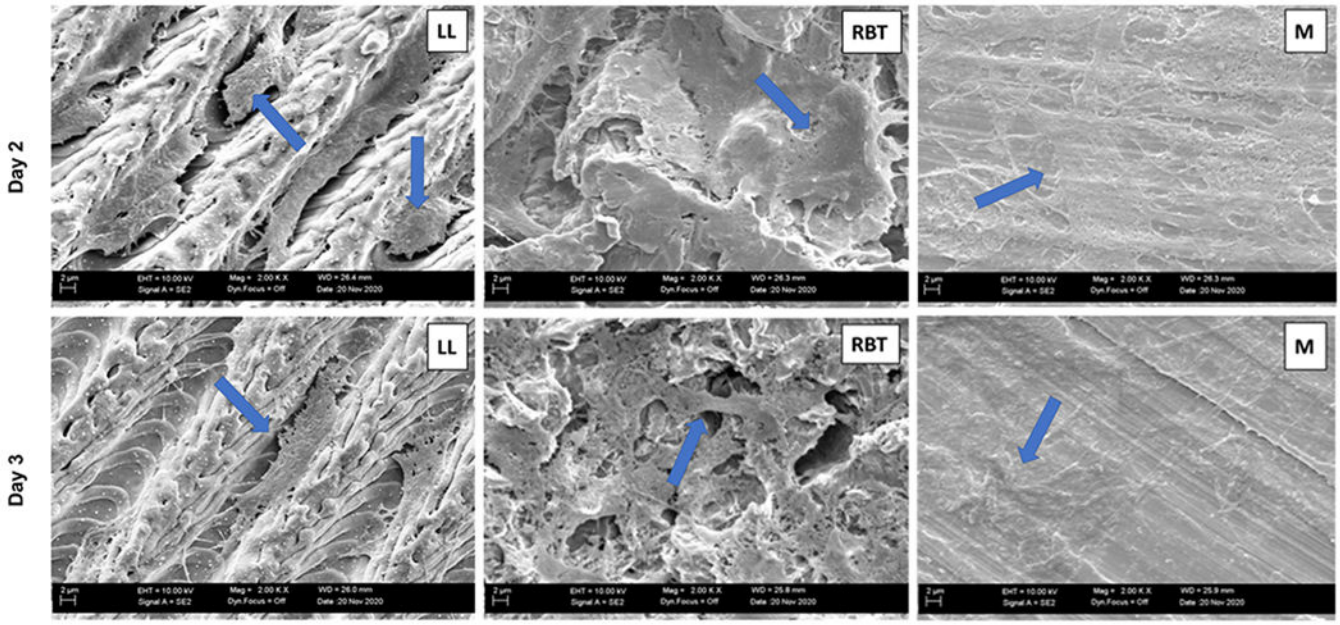

Fig. 8.

Scanning electron microscopy of pre-osteoblasts on representative Laser-Lok (LL), resorbable blast textured (RBT), and machined (M) samples at days 2 and 3 (2000X, scale bar = 2 μm). Arrows indicate cells.

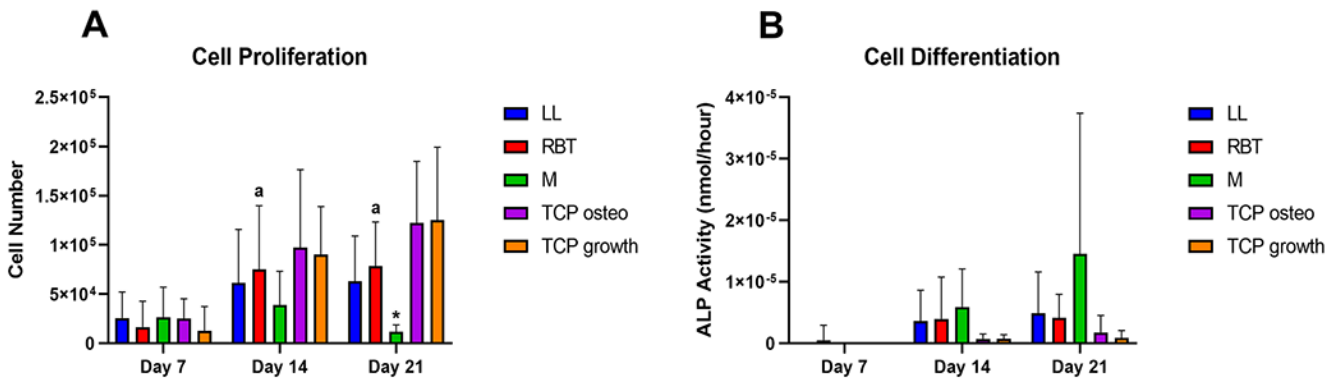

Fig. 9.

(A) Cell number for pre-osteoblasts at days 7, 14, and 21. (*) indicates significant difference to all other groups within the time point, (a) indicates significant difference to day 7 within that group ($p<0.05$). (B) Alkaline phosphatase (ALP) activity at days 7, 14, and 21 (note: log scale). There were no significant differences ($\alpha=0.05$) between groups. Sample sizes: day 7 (n = 6–14), day 14 (n = 5–14), day 21 (n = 6–14).